Southeastern Europe Tunnelling Conference (SETC-2025)
1-3 October 2025, Belgrade, Serbia

DOI: 10.5937/SETC25015K

Prediction and validation of stress-induced rock bursting in a deep Himalayan tunnel through empirical methods

Rahul Khanna[a], Rajeev Anuj Sharma[a] and Ranjit Singh[b]*

[a] NHPC Ltd., Parbati HE Project, Stage-II, Manikaran, Himachal Pradesh, India; rajeev@nhpc.nic.in
[b] NHPC Ltd., Parbati HE Project, Stage-II, Nagwain, Himachal Pradesh, India; ranjit@nhpc.nic.in

Abstract: The deep tunnels under construction in the tectonically active Himalayan terrain endure high magnitudes of field stresses, causing brittle failure. The instability caused by the tunneling media is manifested in the form of spalling and rock bursts. This paper focuses on determining the yielding capacity of the stressed rock strata through RMR-14 employing elastic behaviour index (ICE) and stress factor (Fs). The ratio of far-field maximum stress to compressive strength is used to evaluate tunnel stability. The rock-bursting potential is determined from the tangential stress components in the roof and side walls of the tunnel. The competency factor (C_g) for the brittle quartzite is also estimated. The results are validated for a 1.2 km stretch of the 31.56 km long head race tunnel of the Parbati 2 hydroelectric project. An innovative chart-based technique is developed for field recording of stress-induced incidents based on their severity, duration, periodicity, and impact on the tunnel profile. The back analysis indicates those reaches that witnessed frequent incidents of violent rock bursting and faced difficulty providing rock support have a ratio of maximum boundary stress (σ_1) and compressive strength (σ_c) greater than 0.5, C_g less than 1.0, and ICE ≤15. Results indicate that ICE is a handy tool for predicting the stress-deformation characteristics.

Keywords: rock burst; elastic behaviour index; competency factor; compressive strength

1. Introduction

The young and dynamic Himalayas present unusually challenging ground conditions during the construction of deep-seated transport and hydro tunnels. A prudent and thorough understanding of the expected geology, along with an unambiguous prediction of the stress-deformation characteristics of the rock mass, is crucial to the success of these tunneling projects. Failures in deep tunnels are a function of intact rock strength, joint distribution, and the magnitude and direction of in-situ stresses. Stress-induced fractures developed around the excavation boundary are termed as brittle failure (Hoek et al., 1995). When a deep-seated tunnel passing through hard and brittle rocks intercepts regions of high field stresses, localized brittle failures accompanied by the sudden release of elastic strain energy are observed (Palmström, 1995; Feng, 2017; Cai and Kaiser, 2018; Askaripour et al., 2022). Such failures are manifested as rock spalling, slabbing, and rock bursting (Ortlepp and Stacey, 1994). Several researchers have attempted to predict the phenomenon of rock bursting in deep mines and hydro tunnels through various techniques, such as empirical methods (Russenes, 1974; Barton et al., 1974; Palmström, 1995; Diederichs, 2007; Russo, 2014; Farhadian, 2021), machine learning and artificial neural network techniques (Zhang et al., 2020; Zhao et al., 2021), micro seismic monitoring (Jenkins et al., 1990; Kasier and Maloney, 1997; Urbancic et al., 2000; Shen et al., 2008; Ma et al., 2021) and numerical modelling techniques (Miranda, 1972; Hart, 1980; Zubelewicz and Mroz, 1983; Jing and Hudson, 2002; Cai et al., 2007; Wang and Cai, 2017; Gao, 2019). Numerical methods generally have limitations in considering factors and criteria. Micro seismic monitoring faces issues like elastic wave signal overlap, quantifying indicator sensitivity, and unreliable warning time. Machine learning methods exhibit good predictive ability but are limited by the quality of input indicators, the size of sample datasets, and data processing issues. On the other hand, accurate measurement of in situ field stresses is very cumbersome, as stress is a tensor quantity that varies in magnitude and direction in

*Corresponding author: rahul@nhpc.nic.in (R. Khanna).

three-dimensional space. Moreover, the complexity, discontinuity, and inhomogeneity of the rock mass also limit the possibility of its accurate measurement (Amadei et al., 1997). Experience with in-situ tests also suggests an inconsistency in results and variations within proximity (Dev, 2019). Moreover, in the ongoing construction projects, due to very hard-pressing schedules, it is not possible to carry out field tests as they are expensive and require dedicated, undisturbed space. Alternatively, understanding the instability of tunnels due to in-situ stress-deformation behavior and the reliable prediction of rock bursting through empirical relations offers a convenient and straightforward approach. This paper predicts stress-deformation behaviour for a 1.2 km reach of the 31.5 km long head race tunnel of the Parbati 2 hydroelectric project. Additionally, a chart-based technique devised for recording stress-induced conditions during tunneling is also presented.

2. About the project layout and geology

The Parbati 2 hydroelectric project, with an installed capacity of 800 MW, falls in the Kullu district of Himachal Pradesh, India. This project of national importance is owned by NHPC Ltd., a Government of India undertaking. It involves inter-basin transfer of water from Parbati to the Sainj River (Fig. 1). A gross head of 862.5m is utilized for the generation of 3124.6 GWH of annual energy in a 90% dependable year. Commercial operation commenced after the commissioning of all four 200 MW units each during March and April 2025. The head race tunnel is a pressurized tunnel with maximum and minimum static water heads of 1.07 bars and 7.9 bars at the downstream and upstream ends, respectively. The 31.56 km long and 6m diameter tunnel has a gradient of 1:461.6 carrying a design discharge of 116 m^3/sec with an average velocity of 4.10 m/sec. The maximum and minimum vertical cover above the tunnel are 1683 m and 123 m, respectively. About 5.7 km of the tunnel, which is excavated using an open shield Tunnel Boring Machine (TBM), is circular, while the remaining portion, excavated by the conventional drilling and blasting method, is horseshoe-shaped.

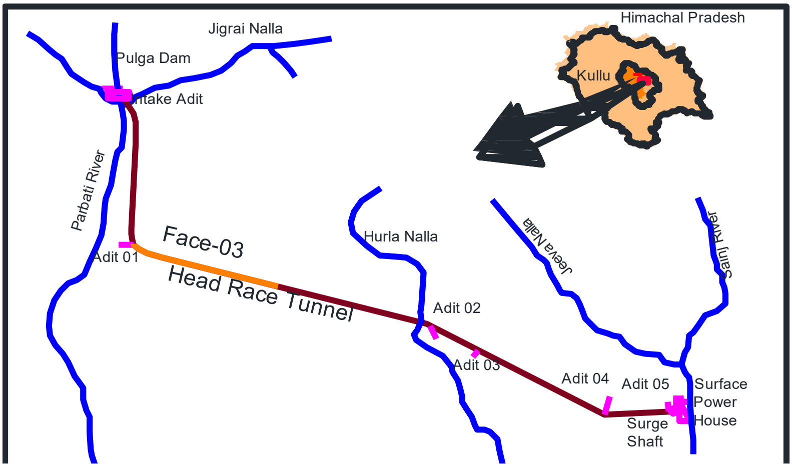

Fig. 1. Project layout showing head race tunnel alignment.

The project is located within the "Kullu Window" of the Lesser Himalayas, comprising crystalline and metasedimentary rocks of the Kullu and Rampur Groups, including granitic gneiss, mica gneiss, biotite and quartzite schist, quartzite, slate, phyllite, and dolomite. A major fault system structurally bounds the area, specifically the Main Central Thrust (MCT), and has undergone intense deformation, resulting in the formation of several faults, folds, shear zones, and intense jointing of the rock strata. The 5608 m tunnel section along the downstream face-03 discussed here was excavated from adit 01, starting from chainage 6364 m to 11385 m. The rock types encountered were biotite mica schist with quartzite, phyllite with carbonaceous phyllite, quartzite with bands of schists, and chlorite schists (Fig. 2). A faulted contact was intercepted around chainage 9684 m between carbonaceous phyllites and quartzites.

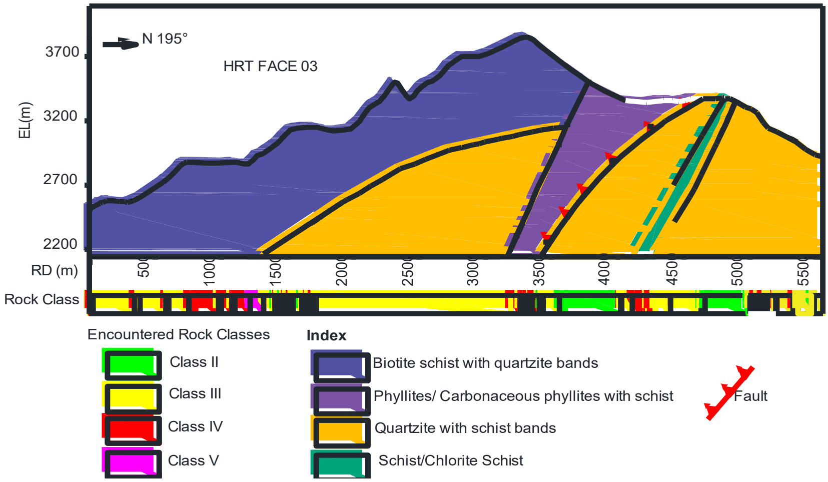

Fig. 2. Geological L-Section along head race tunnel (face 03) and encountered rock classes.

3. Prediction of stress-deformation characteristics through empirical methods

The deformation and rock burst potential in a deep tunnel can be predicted through a profound understanding of stress conditions and compressive strength of the rock mass using empirical correlations. Quantitative rock mass characterization systems such as RSR (Wickham et al., 1972), RMR (Bieniawski, 1973, 1989), Q-system (Barton et al., 1974), and RMi (Palmström, 1995) have been empirically developed utilizing rock mass data from various civil engineering projects with an attempt to incorporate most of the engineering geological parameters (Hoek, 2004). However, each system has its limitations in defining the holistic behavior of rock mass, considering that only limited input data sets have been utilized. RSR and RMR_{89} systems do not offer any means to evaluate the stress conditions of the rock mass.

3.1. Elastic Behavior Index (ICE)

Celada et al. (2014), based on 2,298 case histories, updated the most widely used RMR89 and came out with an improvised RMR14 system having five basic parameters and three adjustment factors, including stress factor (Fs) to consider stress-deformation behavior of the rock mass by employing "*Índice de Comportamiento Elástico*" referred to as ICE (Bieniawski et al., 2011) or Elastic Behavior Index, which is defined as:

$$Ko \leq 1:\ ICE = \frac{3704\sigma c * e^{\frac{RMR-100}{24}}}{(3-Ko)*H} * F \tag{1}$$

$$Ko \geq 1:\ ICE = \frac{3704\sigma c * e^{\frac{RMR-100}{24}}}{(3Ko-1)*H} * F \tag{2}$$

Where σ_c is the uniaxial compressive strength of the intact rock in MPa; Ko is the ratio of horizontal to vertical stresses; H is the tunnel depth in m, and F is the shape coefficient, considered as 1 for a 6 m diameter horseshoe-shaped tunnel. RMR above is corrected for discontinuity orientation. From ICE, the stress-deformation behavior of the tunnel is determined (Table 1). Excavation having an ICE < 70 exhibits stress-induced conditions. The stress factor (Fs) aims to account for the declining impact of yielding in the tunnel and is estimated from ICE (Mateus et al., 2023). Celada et al. (2014) showed that stress factor (Fs) ranged between 0 to 1.3. Fs is 1 for ICE>70 and 1.3 for ICE<15. The Fs values for the 1.2 km tunnel reach from Adit-1 plotted on the ICE-Fs curve (Fig. 3) indicate the stress-deformation condition, which has been predicted as mostly yielding to moderately yielding (ICE<50).

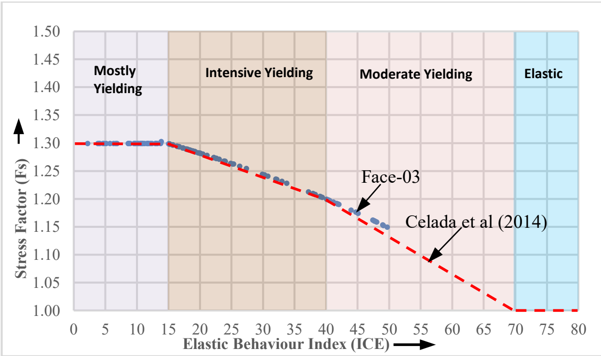

Fig. 3. Stress Factor (Fs) estimated for the 1.2km HRT reach plotted on the ICE-Fs of Celada et al. (2014).

Table 1. Stress-deformation behaviour as a function of ICE (Celada et al., 2014).

ICE	Stress-deformation behavior
>130	Completely elastic
70-130	Elastic with incipient yielding
40-69	Moderate yielding
15-39	Intensive yielding
<15	Mostly yielding

3.2. Hoek and Brown stability classes

Intact rock uniaxial compressive strength (σ_c) used in this study is measured in the field using an N-type Schmidt hammer. The rebound numbers (RN) are collected in the field according to the procedure outlined in the "ISRM Suggested Method" (Aydin, 2009). The UCS is estimated using the empirical equation (Bolla and Paronuzzi, 2021):

$$\sigma_c = 5.2251 * e^{(0.0449\ RN)} \tag{3}$$

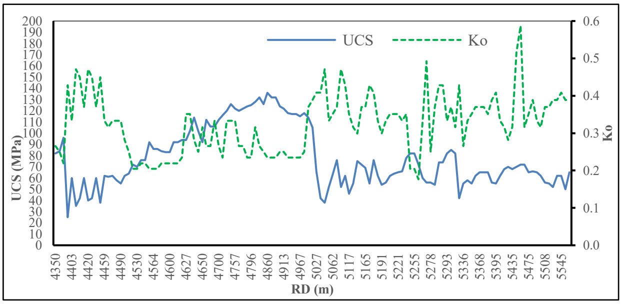

Fig. 4. RD-wise plot of compressive strength (σ_c) and stress ratio (Ko).

The vertical stress (σ_v) is calculated in MPa from the relation given by Hoek and Brown (1980)

$$\sigma v = 0.027 * z \tag{4}$$

Where z is the depth of the overburden. The horizontal-to-vertical stress ratio (K0) is considered as a function of the Poisson's ratio (μ) estimated from the tunnel seismic prediction using primary and shear wave velocities Vp and Vs using the expression Vp2-2Vs2/2(Vp2-Vs2). An RD-wise plot of K0for

Face 03 is shown in Fig. 4. The maximum and minimum horizontal field stresses (σ1 and σ3) are estimated using relations proposed by Stephansson (1993) for z<1000m.

$$\sigma_1 = \sigma_H = 2.8 + 1.48 * \sigma_v \quad (5)$$

$$\sigma_3 = \sigma_h = 2.2 + 0.89 * \sigma_v \quad (6)$$

The tangential stresses around the tunnel opening are estimated using the relation (Hoek and Brown,1980):

For the tunnel roof: $\sigma_{\theta r} = (A \times Ko - 1) * \sigma_v$ (7)

For side walls: $\sigma_{\theta w} = (B - Ko) * \sigma_v$ (8)

Where A and B are excavation geometry factors whose values are 3.2 and 2.3, respectively, for horseshoe-shaped tunnels. Hoek and Brown (1980) based on the observations made in South African mines suggested that for a stress environment where the ratio of maximum to minimum far-field stress (Ko) is equal to 0.5, the stability of underground excavations could be determined from the ratio of far-field maximum stress (σ1) and uniaxial compressive strength of intact rock (σc). The stability classes are shown in Table 2.

Table 2. Hoek and Brown (1980) stability classification.

σ_1/σ_c	Stress Condition	Support required
< 0.2	Stable	Unsupported
0.2-0.3	Minor spalling	Light support
0.3-0.4	Severe spalling	Moderate support
0.4-0.5	Rock bursting	Heavy support
> 0.5	Heavy/violent rock bursting	Difficult to support

Tunnel stability prediction (Hoek and Brown, 1980), as shown in Fig. 5, indicates that almost the entire tunnel reach beyond RD 4975m is prone to rock bursting.

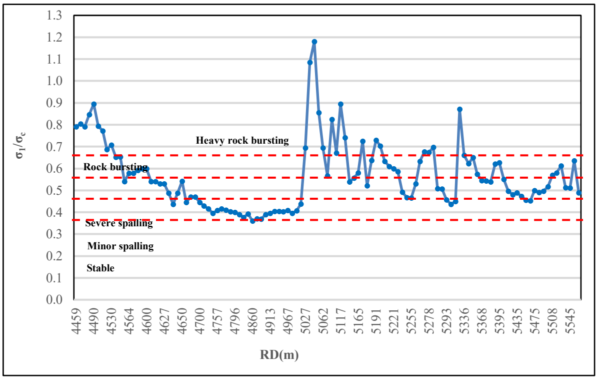

Fig. 5. RD-wise plot of (σ_1/σ_c) ratio along the tunnel.

3.3. Competency Factor (Cg)

RMi (Palmstrom, 1995) defines the “Competency Factor” (Cg) as the ratio of compressive strength and tangential stress to ascertain the rock-bursting potential:

$$Cg = RMi/\sigma_\theta = f_\theta \ x \ \sigma_c/\sigma_\theta \approx 0.5 \ x \ \sigma_c/\sigma_\theta \tag{9}$$

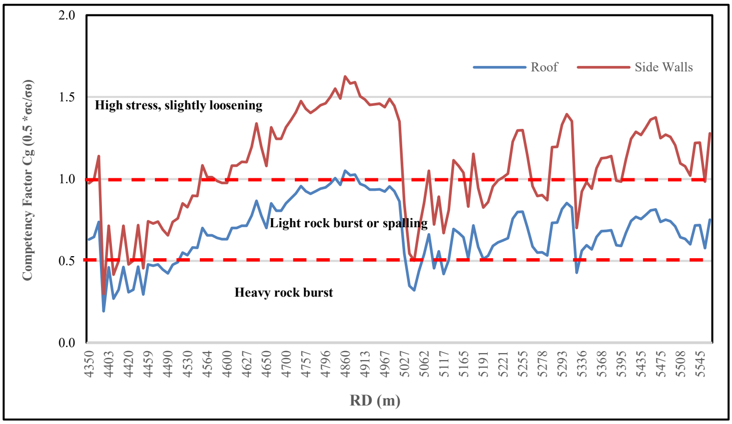

Fig. 6. The plot of the competency factor for tunnel roof and side walls.

For C_g > 2.5: No rock stress-induced instability; C_g =2.5-1.0: High stress, slightly loosening; C_g =1.0-0.5: Light rock burst or spalling, and Cg< 0.5: Heavy rock burst. The Competency factor (Cg) for the tunnel roof and side walls separately has been plotted for the head race tunnel under study (Fig. 6). The plot indicates that most of the tunnel reach beyond RD ±4975m has been predicted as prone to light to heavy rock bursting or rock spalling. The above prediction for stress-induced stability performed through various empirical methods has been validated with the actual incidents of rock bursting witnessed in the 1.2 km reach of HRT face 03.

4. Incidents of Rock-bursting at Parbati Hydroelectric Power Project, Stage-2

In this study, a 1.2 km horseshoe-shaped reach of HRT from the Adit-1 side, excavated through complexly jointed, hard, and brittle quartzite with bands of quartzite schist/mica-schist, is examined. The superincumbent cover varied from 1182m to 724m. A few rock bursts are discussed below, where significant time was consumed for providing stabilization measures. Two violent rock bursts occurred around RD ±5072m, followed by the ingress of a large quantity of muck (~800 m³) and groundwater (~300 l/min), resulting in the formation of a cavity. Ingressed muck/slush spread into the tunnel up to ±60m behind the face, burying the drill-jumbo (Fig. 7). The cavity was negotiated by carrying out extensive cement grouting, channelizing seepage through drainage holes, and by providing two sets of pipe roofing umbrellas beside forepoling, etc.

(a) (b) (c)

Fig. 7. (a) Formation of cavity due to rock bursts; (b) The flow of muck, slush, and groundwater ingress from the cavity; (c) Filling of the tunnel by muck and slush and burial of the drill jumbo.

Incessant rock spalling occurred between RD 5090m to 5106m during the mechanical removal of undercut when the muck suddenly erupted from the left wall and invert, followed by violent rock bursting from the face. Episodes of violent rock bursting continued after the blast taken at face, causing a sudden eruption of rock fragments from the crown and exposing all fore poles (Fig. 8a). Multiple violent rock bursts took place from the face and left crown at RD ±5240m just after completion of face drilling. The incident started with minor popping sounds followed by sudden rock bursts, resulting in spalling of rock fragments up to 6-8m. Later on, intermittent rock bursting continued about 15 to 18m behind the face from the left wall and invert, resulting in the eruption of rock fragments and detachment of rock anchors and shotcrete already applied (Fig. 8b).

On several occasions, already installed support has been disrupted due to severe rock bursts. As the tunnel got further excavated, two more major incidents of violent rock bursts happened around RD ±5284m and RD ±5297m towards the right wall and crown just after the face blast in the supported area. The incidents started with minor popping, followed by a heavy blast-like sound and spalling of rock fragments all over the area. The rock anchors got exposed while SFRS was detached from the tunnel surface due to rockfall (Fig. 9a). Recurring rock bursts around RD ±5352m resulted in rockfall and detachment of shotcrete and rock anchors. The rock bursts were so severe that fragments around 0.5 to >1.0m in size were thrown away from the face up to the operator's chamber of the drill jumbo. The above incidents resulted in the enlargement of the tunnel section (Fig. 9b).

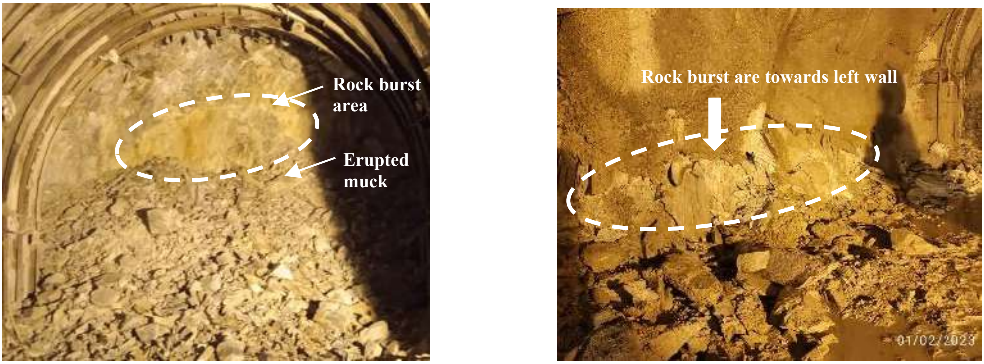

(a) (b)

Fig. 8. (a) Impact of intermittent and violent bursts at face around RD 5106m; (b) Multiple rock bursting from 18-15m behind the face around RD 5240m.

(a) (b)

Fig. 9. (a) Rock spalling resulted in detachment of shotcrete and rock anchors around RD ±5284m; (b) Fore poles detached and hanged after multiple episodes of rock bursts at the face and crown around RD ±5352m.

5. Stabilization and Support Measures

Normal rock support such as rock anchors, shotcrete with wire mesh, and steel rib sets with pre-cast concrete laggings, were provided depending on the rock class. In order to arrest the persistent rock bursting, support measures were required to be provided timely such that significant time is not lost. Therefore additional support measures were implemented for rock burst reaches. The layer-wise application of steel fiber reinforced shotcrete (SFRS) has been very useful. For stabilizing the face, SFRS, as well as normal shotcrete of thickness up to 100 mm, has been applied using a CIFA shotcrete spraying machine (Fig. 10a), besides keeping the face idle for redistribution of stresses.

Fig. 10. (a) Application of normal shotcrete and SFRS layer-wise on tunnel face, crown, and side walls; (b) Drilling of stress relief holes (SRH) at the face using a double boom drill jumbo.

When the rock fall has been arrested, rock anchors were installed. Stress relief holes (SRH) were drilled to destress the rock mass. Two to six SRH have been drilled, having 76 mm diameter and a length up to 6m on the face after every blast in the above tunnel reach (Fig. 10b). Cumulatively, about 4388m of drilling for SRH has been undertaken. To ensure the safety of men and machinery, it was felt prudent to provide steel ribs with steel lagging in rock-bursting reaches after spraying shotcrete. The drilling jumbo was retrofitted with a protective wire mesh screen to prevent the drilling crew from being hurt.

The influence of providing appropriate stabilization measures is evident through a comparative analysis of excavation cycle time (Fig. 11). The cycle time has significantly reduced from more than 72 hrs. to 15-20 hrs. in the tunnel reaches affected by incidents of violent rock bursting. Beyond RD 5250 m, the SRHs were provided on a progressive basis by making them part of the excavation cycle. The quantity of explosives during the face blasting was also controlled such that the pull is limited only up to 2-2.5m. These efforts have affected the intensity and frequency of the rock bursting to a greater extent.

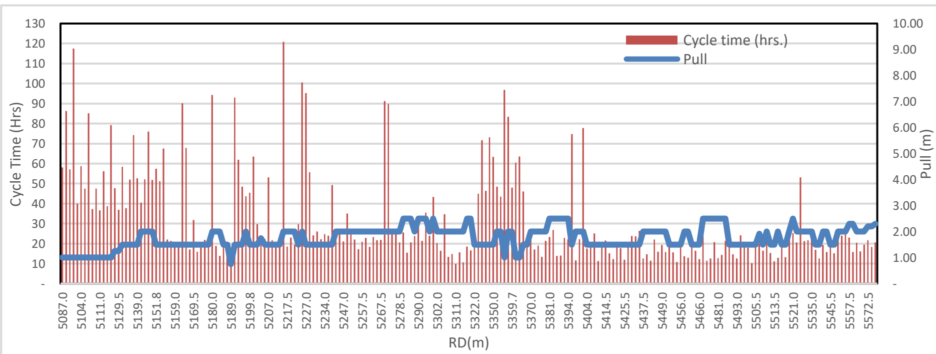

Fig. 11. RD-wise plot of cycle time and pull along head race tunnel face 03.

6. Validation and back analysis

Based on the Norwegian rule of thumb, a tunnel is likely to experience stress-induced rock bursts once the superincumbent cover exceeds 500m, and the severity of such incidents increases if the tunnel runs parallel to the valley side with a slope angle exceeding 25 degrees (Selmer-Olsen, 1965). Almost the entire head race tunnel reach considered in this study exceeds the above-mentioned threshold. Therefore, it is necessary to evaluate the stress-induced condition using more advanced empirical methods. For this purpose, the latest version of the rock mass rating system (RMR_{14}) developed by Celada et al. (2014) has been considered. It is an update of RMR_{89} (Bieniawski, 1989). An excellent correlation has been worked out between RMR_{89} and RMR_{14} for a 1226m stretch for the head race tunnel along the face 03, based on about 152 data points for $20 \leq RMR_{89} \leq 80$ (Fig. 12).

$$RMR_{14} = 1.22\ RMR_{89} + 2 \tag{10}$$

The above expression has a value of determination coefficient (R^2) as 0.97 and a correlation coefficient (R) equal to 0.985, thus indicating a strong correlation. The above relation shall be further implemented for the other portion of the head race tunnel as well in future studies.

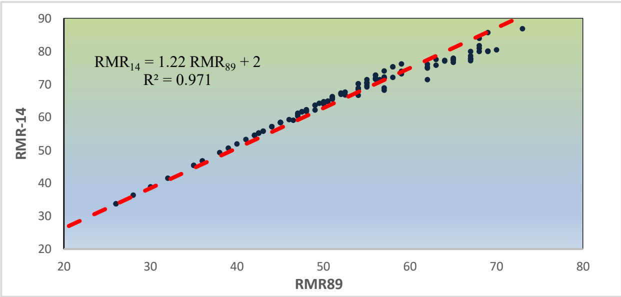

Fig. 12. The plot showing RMR_{89}-RMR_{14} correlation developed for the head race tunnel along face-03.

RMR 14 incorporates a stress factor (Fs) and Elastic Behavior Index (ICE) for the assessment of the stress-deformation behavior of rock mass. For ICE<70, substantial deformation in the rock mass is expected. For ICE< 15, the excavated rock mass is prone to brittle failures (Bieniawski and Celada, 2011). For the entire 1.2 km tunnel reach, RMR-14, Fs, and ICE values are estimated. The RD-wise plot of ICE along with rock cover (Fig. 13) shows that most of the rock bursting incidents fall in the intensive to mostly yielding zones with a higher possibility of rock bursting. From RD ±5025m onwards in the detoured part of HRT, the ICE value drops invariably below 15, thus indicating an increased possibility of stress-induced incidents.

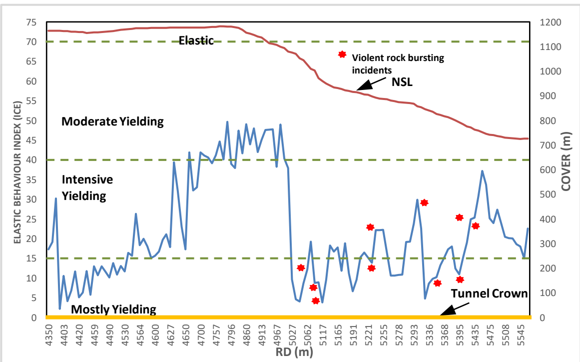

Fig. 13. The RD-wise plot of ICE and rock cover(h).

Further, all the major rock-bursting incidents discussed above are plotted (SC-4 to SC-5 category as per observational stress conditions) in the ICE curve coincides with lower ICE values (ICE<15), indicating high rock-bursting potential (Table 3).

Table 3. Assessment of rock-bursting potential (Celada et al., 2014).

RD (m)	Ko	ICE	RMR-14	Deformation Behavior	SC_{ob}
5069-5074	0.35	12.12	53.30	Mostly yielding	SC-4
5090-5106	0.43	08.92	41.60	Mostly yielding	SC-4
5225-5240	0.33	13.83	61.25	Mostly yielding	SC-5
5280-5284	0.37	10.85	58.50	Mostly yielding	SC-5
5297-5310	0.37	29.88	72.19	Intensely yielding	SC-4
5349-5352	0.33	09.76	52.00	Mostly yielding	SC-5
5394-5396	0.41	10.90	54.60	Mostly yielding	SC-5

Further, the conventional methodology proposed by Hoek and Brown (1980) for determining the stability of underground excavations using the ratio of far-field maximum stress (σ_1) and uniaxial compressive strength of intact rock (σ_c) is also applied for validating the tunnel reaches that witnessed heavy to violent rock burst tunnel (Fig. 14). It is evident that for all the major incidents of rock bursting, the σ_1/σ_c ratio is higher than 0.5 thus indicating severe to very severe rock bursting potential (Table 4).

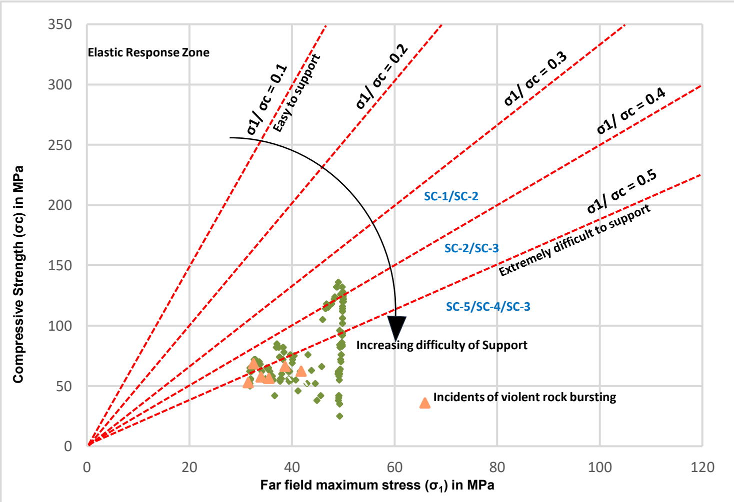

Fig. 14. The σ_1-σ_c plot shows the stability classes of Hoek and Brown (1980). The values for HRT are plotted. The triangles shown are violent rock-bursting reaches.

Table 4. Assessment of rock-bursting potential (Hoek and Brown, 1980).

RD (m)	σ_c	σ_1	σ_2	σ_3	σ_1/σ_c	Risk of violent rapture
5069-5074	63	43.7	27.6	26.8	0.69	Very severe
5090-5106	62	41.6	26.2	25.5	0.67	Very severe
5225-5240	66	38.4	24.2	23.7	0.59	Very severe
5280-5284	54	37.6	23.5	23.1	0.70	Very severe
5297-5310	85	37.0	23.1	22.8	0.44	Severe
5349-5352	55	34.4	21.2	21.2	0.63	Very severe
5394-5396	70	33.6	20.8	20.7	0.48	Severe

7. Observation-based recording of rock bursts

In tunneling projects, stress-induced deformations are monitored using geotechnical instrumentation. Besides, systematic recording of stress-induced incidents in deep tunnels that happen abruptly is also very useful. This information not only helps during back analysis and validation of the prediction but also assists in timely decision-making for undertaking appropriate stabilizing measures for safe excavation. With the above intent, an innovative chart-based technique is developed in this study for field recording, where the stress-induced conditions are categorized into five types: SC-1, SC-2, SC-3, SC-4, and SC-5. This categorization is based on the observed intensity, duration of occurrence, periodicity, sounds produced, and instability caused by the failure of the rock mass and its location (Table 1). Based on the above five stress-induced conditions, an assessment of their impact on the tunnel profile is also documented from the observational experience in tunnels (Table 5).

Table 5. Description of observation-based stress conditions in the head race tunnel.

Type	Intensity	Duration (Periodicity)	Sounds	Rock spalling/ Rockfall
SC-1	Very Mild	A few seconds (once or twice)	Popping	Nil
SC-2	Mild	From a few seconds up to one minute (continuous)	Popping /rapture	Nil
SC-3	Moderate	From a few seconds up to more than one minute (once, twice, intermittent)	Popping/ rapture/ mild blast	One, two or more incidents of minor rock spalling.
SC-4	Moderate to Violent	More than one minute (intermittent)	Rapture/ heavy blast	Multiple incidents of rock spalling/rockfall from several locations.
SC-5	Violent to intensely Violent	One minute to more than five minutes (continuous)	Rapture/ violent blast	Incessant rock burst/ rock fall/ shooting rock fragments from several locations.

Based on the above five stress-induced conditions, an assessment of their impact on the tunnel profile is also documented from the observational experience in tunnels (Table 6). SC-1 type incidents are very mild and have no impact on the tunnel profile. In contrast, SC-5 type incidents are characterized by heavy and violent rock bursting, resulting in rockfalls and enlargement of tunnel sections. The above technique has been extensively applied during the construction of the 1.2km stretch of the head race tunnel of the Parbati hydroelectric project, stage II excavated by the drilling-blasting method (DBM). Progressive recording of all stress-induced incidents, activity-wise, daily during each shift, has been made. More than 250 stress-induced incidents, ranging from mild popping to violent rock bursting, have been recorded during the excavation. An observation chart is prepared wherein each incident defined in Table 5 above has been recorded activity-wise (face drilling, loading, blasting, defuming, mucking, scaling, drilling of pressure relief holes, rock anchoring, shotcreting, and other support installation) throughout the cycle time in each shift. The rock mass rating (RMR) and location of the incident (left wall, crown, and right wall) are also indicated.

Table 6. Impact of stress condition on profile.

Type	Impact on the Tunnel profile
SC-1	None
SC-2	None to minor overbreak during scaling due to loosening/ opening of joints
SC-3	A few rock blocks may detach, causing a minor overbreak in the crown
SC-4	Detachment of blocks along joints, resulting in the enlargement of the tunnel section in the crown; minor to moderate overbreak towards the side walls
SC-5	Significant overbreak in crown and side walls. Rockfall/ spalling from the tunnel face may lead to face collapse.

Based on the above recording, all stress-induced incidents are plotted activity-wise (Fig. 15). The following inferences are drawn from the above plot:

1. Most incidents occurred when the face was disturbed, i.e., either during drilling of blast holes or pressure relief holes, or scaling and undercut removal.
2. Several mild to moderate incidents (SC-1 to SC-4) have occurred in Class-IV rock mass (RMR≤40). This is contrary to the belief that such failures occur only in good-quality rock.
3. The majority of stress-induced incidents have occurred towards the left wall and crown.
4. A significant number of incidents have occurred during the installation of rock supports. This has extended the cycle time of tunnel excavation.

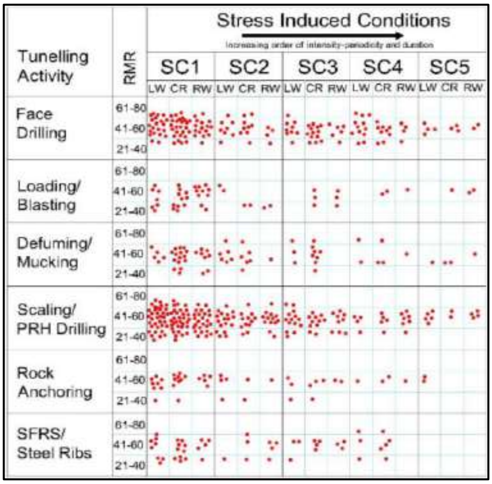

Fig. 15. Chart-based recording of stress-induced condition for a 1.25 km long stretch of HRT Face 03.

8. Conclusions

The prediction of stress-deformation behaviour for a selected portion of the HRT Face 03 from the Parbati 2 hydroelectric project suggests that a significant tunnel reach exhibits ICE≤40, indicating brittle failure. The back calculation of ICE for rock burst areas ranged between 9.76 to 13.83, indicating a very high potential. The (σ_1/σ_c) ratio ranges between 0.44 to 0.69, indicating severe to very severe risk of violent rock bursting and extremely difficult conditions for support installation. The competency factor (C_g) ranges between 0.49 to 0.85 for tunnel crown and 0.69 to 1.03 for side walls, predicting the possibility of moderate to heavy rock bursting. In deep tunnels, the scientific recording of rock bursts is significantly important. This study proposes an observation-based method that considers activity-wise recording of stress-induced conditions based on their intensity, duration, periodicity, sound, and nature of rockfall. Their impact on the tunnel profile is also discussed. The recorded data suggests that most rock-bursting incidents occurred when the face was disturbed during face drilling, scaling, undercut removal, etc. It is also inferred that some severe incidents occurred not only in hard and brittle quartzites but also in low-quality schistose quartzite/mica schist with RMR≤40. Keeping the face idle for some time, followed by drilling stress relief holes and the layer-wise application of SFRS, has helped control rock bursting. The application of the prediction and recording methodology suggested in this study shall help in keeping advanced provisions in contracts of future tunnelling projects for stabilization measures to arrest stress-induced spalling and rock bursts. Finite element and discrete numerical modelling techniques shall also be applied in future studies to validate the rock bursting potential of deep tunnels.

Acknowledgments

The authors thank NHPC management for granting permission to present and publish this work.

References

Amadei, B., Stephansson, O., 1997. Rock Stress and Its Measurement. Springer, Berlin.

Askaripour, M., Saeidi, A., Rouleau, A., Mercier-Langevin, P., 2022. Rock burst in underground excavations: A review of mechanism, classification, and prediction methods. *Underground Space*, 7 (4): 577-607.

Aydin, A., 2009. ISRM suggested Method for Determination of the Schmidt Hammer Rebound Hardness: Revised Version. *International Journal of Rock Mechanics and Mining Sciences*, 46: 627-634.

Barton, N.R., Lien, R., Lunde, J., 1974. Engineering Classification of Rock Masses for the Design of Tunnel Support. *Rock Mechanics*, 4:189-239.

Bieniawski, Z.T., 1973. Engineering Classification of Jointed Rock Masses. *Civil Engineering*, 12: 335-343.

Bieniawski, Z.T., 1989. Engineering Rock Mass Classification: A Complete Manual. New York, John Wiley and Sons: 251.

Bieniawski, Z.T., Celada, B., Aguado, D., Rodríguez, A., 2011. Forecasting tunnelling behaviour. *Tunnels & Tunnelling*. August 2011, 39-42.

Bolla, A., Paronuzzi, P., 2021. UCS field estimation of intact rock using the Schmidt hammer: A new empirical approach. IOP Conference Series: Earth and Environmental Science, 833(1): 012014

Cai, M., Kaiser, P. K., Morioka, H., Minami, M., Maejima, T., Tasaka, Y., Kurose, H., 2007. FLAC/PFC coupled numerical simulation of AE in large-scale underground excavations. *International Journal of Rock Mechanics and Mining Sciences*, 44(4): 550–564.

Cai, M., Kaiser, P.K., 2018. Rock burst phenomena and support characteristics. In: Rock burst Support Reference Book, I. Laurentian University, p. 191.

Celada, B., Tardaguila, I., Varona, P., Rodriguez, A., Bieniawski, Z.T., 2014. Innovating tunnel design by an improved experience-based RMR system. World Tunnel Congress, Iguassu Falls, Brazil.

Diederichs, M.S., 2007. The 2003 Canadian Geotechnical Colloquium: Mechanistic interpretation and practical application of damage and spalling prediction criteria for deep tunnelling. *Can. Geotech J.*, 44:1082–1116.

Farhadian, H., 2021. A new empirical chart for rock burst analysis in tunnelling: Tunnel rock burst classification (TRC), *International Journal of Mining Science and Technology*, 31 (4): 603-610.

Feng, X., Liu, J., Chen, B., Xiao, Y., Feng, G., Zhang, F., 2017. Monitoring, warning, and control of rock bursts in deep metal mines. *Engineering* 3:538-545.

Gao, F., 2019. Use of numerical modeling for analyzing rock mechanics problems in underground coal mine practices. *J. Min. Strata Contr. Eng.* 1 (1): 013004

Dev, H., 2019. Evaluation of in-situ stresses in Rock Mass: Challenges and Applications in Hydropower Development, *Journal of Rock Mechanics & Tunnelling Technology*, 25 (2): 103-112.

Hart, R.D., 1980. Geotechnical modelling of a cut and fill mining operation. In: Proceedings of the Conference on the Application of Rock Mechanics to Cut and Fill Mining. Lulea. Institute of Mining and Metallurgy, Sweden: 307-315.

Hoek, E., Brown, E. T., 1980. Underground Excavations in Rock. The Institution of Mining and Metallurgy, London.

Hoek, E., Kaiser, P. K., Bawden, W. F., 1995. Support of underground excavations in hard rock. Rotterdam, Netherlands: A. A. Balkema Publishers.

Hoek, E., 2004. Rock mass classification. Practical Rock Engineering, 2023 Ed., Rocscience.

Jenkins, F.M., Williams, T.J., Wideman, C.J., 1990. Rock burst mechanism studies at the Lucky Friday Mine. Proceedings of the 31st U.S. Symposium on Rock Mechanics. WV University, Rotterdam: Balkema: 955–962.

Jing, L., Hudson, J.A., 2002. Numerical methods in rock mechanics. *Int. J. Rock Mech. Min. Sci.* 39 (4): 409-427.

Kasier, P.K., Maloney, S.M., 1997. Ground motion parameters for design of support in burst-prone ground. In: Gibowicz and Lasocki, editors. Rock bursts and seismicity in mines. Rotterdam: Balkema. pp. 337–342.

Ma, T. H., Tang, C. A., Liu, F., Zhang, S. C., Feng, Z. Q., 2021. Micro seismic monitoring, analysis and early warning of rock burst. Geomatics. *Natural Hazards and Risk*, 12(1): 2956–2983.

Mateus, S., Afonso, M.J., Fernandes, I., Chaminé, H.I., 2023. RMR14 versus RMR89: A methodological approach for rock mass excavations (N Portugal). Advances in Geoengineering, Geotechnologies, and Geoenvironment for Earth Systems and Sustainable Georesources Management. Advances in Science, Technology & Innovation. Springer, Cham: 187–192.

Miranda, E.E., 1972. Deformation and Fracture of Concrete Under Uniaxial Impact Loading (Unpublished PhD Thesis). University of Missouri Rolla, Rolla, USA.

Ortlepp, W.D., Stacey, T.R., 1994. Rock burst Mechanisms in Tunnels and Shafts. *Tunnel and Underground Space Technology*, 91: 59–65.

Palmström, A., 1995. RMi-A Rock Mass Characterization System for Rock Engineering Purposes. PhD Thesis, The University of Oslo, Norway:400.

Russenes, B.F., 1974. Analysis of rock spalling for tunnels in steep valley sides [Unpublished Master's thesis]. Norwegian Institute of Technology.

Russo, G., 2014. An update of the "multiple graph" approach for the preliminary assessment of the excavation behaviour in rock tunnelling. *Tunnel and Underground Space Technology*, 41:74–81.

Selmer-Olsen, R., 1965. Stability of tunnels in valley sides. (In Norwegian), IVA-meddelande, Stockholm, 142: 77-83.

Shen, B., King, A., Guo, H., 2008. Displacement, stress, and seismicity in roadway roofs during mining-induced failure. *International Journal of Rock Mechanics and Mining Science*, 45(5):672–688.

Stephansson, O., 1993. Rock Stress in the Fennoscandian Shield. In Comprehensive Rock Engineering, Pergamon, 3 (17): 445-459.

Urbancic, T.I., Trifu, C.I., 2000. Recent advances in seismic monitoring technology at Canadian mines. *Journal of Applied Geophysics*, 45(4): 225–237.

Wang, X., Cai, M., 2017. Coupled numerical analysis of ground motion near excavation boundaries in underground mines. *Rock Soil Mech.* 38 (11):3347-3354.

Wickham, G.E., Tiedemann, H.R., and Skinner, E.H., 1972. Support determination based on geologic predictions. North American Rapid Excavation Tunnelling Conference, Chicago: 43-64.

Zhao, H., Chen, B., Zhu, C., 2021. Decision tree model for rock burst prediction based on micro seismic monitoring. *Advances in Civil Engineering*, 2021:1–14.

Zhang, L., Zhang, X., Wu, J., Zhao, D., Fu, H., 2020. Rock burst prediction model based on comprehensive weight and extension methods and its engineering application. *Bulletin of Engineering Geology and the Environment*, 79: 4891–4903.

Zubelewicz, A., Mroz, Z., 1983. Numerical simulation of rock burst processes treated as problems of dynamic instability. *Rock Mechanics and Rock Engineering*, 16(4):253–274.